JOURNAL OF GUIDANCE, CONTROL, AND DYNAMICS
Vol. 16, No. 1, January-February 1993

Ground Tests of Magnetometer-Based Autonomous Navigation (MAGNAV) for Low-Earth-Orbiting Spacecraft

Mark L. Psiaki* and Lejin Huang†
Cornell University, Ithaca, New York 14853
and
Stephen M. Fox ‡
Ithaco, Inc., Ithaca, New York 14850

Actual spacecraft data have been used to test two filters that rely solely on magnetometer measurements to determine spacecraft ephemeris. This work proves the potential of a novel autonomous orbit determination scheme. One of the filters is an extended Kalman-type filter. It estimates a position and velocity, and it uses equations of motion to propagate these estimates. The other filter is a batch least-squares filter. It estimates static Keplerian parameters along with magnetometer biases. Tests of these filters involve filtering of magnetometer data followed by comparison of estimated position with position derived from ground-based tracking. Both filters perform well on the MAGSAT spacecraft, achieving accuracies from 4 to 8 km. Tests of the batch filter on the DE-2 spacecraft yield somewhat larger position uncertainties, 17–18 km. Batch filter tests on the LACE spacecraft yield much larger position errors, 120 km. This poor LACE performance can be attributed partly to solar-array-generated low-frequency noise.

I. Introduction

THE objective of this work has been to use real flight data to evaluate a magnetometer-based autonomous spacecraft navigation scheme. This system could be used in low-Earth-orbit applications where system requirements allow low accuracy but demand complete autonomy. The low expense of the system is an attractive feature: it requires only a three-axis magnetometer and computation time on the flight computer. The system works independently of attitude control or attitude knowledge, which makes it attractive as a backup for use during operational anomalies.

Orbit determination is a mature field. Ground-based approaches make use of ranging data and can be very accurate. Efforts have also been made to develop autonomous orbit determination capability. A survey of autonomous navigation up through 1986 is provided in Ref. 1. Some proposed systems use observations of celestial bodies or observations of landmarks on the Earth. The satellite crosslinks method combines such measurements with measurements of range to other satellites whose orbits are to be determined simultaneously. Tai and Noerdlinger[2] describe a system that relies on sensing the Earth, the moon, and the sun; predicted accuracy is better than 1 km. The Global Positioning System (GPS) can be used for semi-autonomous navigation. With an onboard GPS receiver and a computer, a satellite can determine its position and orbit. This is not truly autonomous, however, because it relies on the availability of GPS signals.

Psiaki and Martel[3] introduced the idea of using the Earth's magnetic field to derive spacecraft position information. They showed that, even if the Earth's field were that of a dipole, five of the six Keplerian elements would be observable in one orbit from magnetic field magnitude measurements alone. The unobservable element would be the longitude of the ascending node. They also developed an extended Kalman filter and tested it on one day's worth of data from a simulated truth model that used an eighth-order International Geomagnetic Reference Field (IGRF) model. The result was complete observability and a predicted 1-σ position accuracy of 4 km. The longitude of the ascending node is observable because the main field's dipole axis is canted with respect to the North Pole, which causes it to rotate with respect to inertial space once per day. Additional observability of longitude is provided by the significant longitudinal variations of the main field's higher harmonics. Fox et al.[4] extended this work to include simulated magnetometer noise in their truth model and to explore a range of orbital inclinations (0–98 deg) and altitudes (350–900 km). They achieved positional accuracies from 10 down to 2 km. Their accuracy depended strongly on the accuracy of the magnetometer and moderately on the orbital characteristics.

The present work tests the magnetometer-based orbit determination filter of Refs. 3 and 4 with real flight data. It filters telemetered magnetometer data to estimate the positions of three spacecraft. These position estimates are compared with position information that has been derived from tracking station data. The result is a very realistic test of the magnetometer-based orbit determination scheme.

Additionally, the present work reports on a new magnetometer-based orbit determination filter. It is a batch least-squares filter. It also works only with magnetometer readings. In addition to estimating orbit and position, it estimates magnetometer biases. It has been developed to cope with the poorer quality of the magnetometer data that are available for two of the test spacecraft.

The body of this paper is divided into six sections. Section II describes the two different orbit determination filters, the extended Kalman filter and the batch least-squares filter. Section III describes the three spacecraft (MAGSAT, DE-2, and LACE) whose telemetry and position information have been used to test the filters. Section IV explains the methods used for evaluating the filters. Sections V, VI, and VII present the MAGSAT, DE-2, and LACE performance results, respectively. The paper concludes with a summary of the major findings of the study.

Received Feb. 25, 1991; presented as Paper 91-2725 at the AIAA Guidance, Navigation, and Control Conference, New Orleans, LA, Aug. 12–14, 1991; revision received March 23, 1992; accepted for publication April 15, 1992.

*Assistant Professor, Department of Mechanical and Aerospace Engineering. Member AIAA.
†Graduate Student, Department of Mechanical and Aerospace Engineering.
‡Principal Systems Engineer. Associate Fellow AIAA.

II. Filter Designs

A. Extended Kalman Filter

An extended Kalman filter has been implemented. The square root information filter (SRIF) form of the state/covariance representation has been used for this filter. It works with a state vector that defines position, velocity, and random-walk disturbance forces. Newton's laws and a gravitational model with J_2 effects are used to propagate the state information equation between measurements. A 10th-order spherical harmonic model of the Earth's magnetic field is used during measurement updates of the state information equation. The filter's model of random disturbance statistics has been sized based on typical ballistic coefficients and the variability of the Earth's atmospheric density. Its model of random measurement error statistics has been sized based on typical field model accuracy.

Filter Dynamic Model

The filter's state vector is

$$x = \left[V, \gamma, \xi, r, \theta, \phi, \frac{SC_L}{m}, \frac{SC_D}{m}, \frac{SC_Y}{m} \right]^T \tag{1}$$

where V is inertial speed, γ is flight-path angle (the angle between the inertial velocity and its projection into the local horizontal plane), ξ is heading angle (the angle between local north and the projection of the inertial velocity vector into the local horizontal plane, measured positive for westward heading), r is radial distance from Earth's center, θ is colatitude, ϕ is east longitude, and SC_L/m, SC_D/m, SC_Y/m are partially nondimensionalized mean aerodynamic lift, drag, and side forces, respectively. The last three quantities are inverse ballistic coefficients; S is surface area, m is spacecraft mass, and C_L, C_D, and C_Y are nondimensional lift, drag, and side force, respectively.

The filter's dynamic equations are

$$\dot{V} = -\tfrac{1}{2}\rho(r - R_E)V^2(x_8 + w_2) + \frac{\mu_E}{r^2}\left\{\sin\gamma\left[-1 + \frac{9}{2}J_2\left(\frac{R_E}{r}\right)^2\left(\cos^2\theta - \frac{1}{3}\right)\right] - \cos\gamma\cos\xi\left[\frac{3}{2}J_2\left(\frac{R_E}{r}\right)^2\sin(2\theta)\right]\right\} \tag{2a}$$

$$\dot{\gamma} = \left(\frac{1}{V}\right)\left(\frac{1}{2}\rho(r - R_E)V^2(x_7 + w_1) + \frac{\mu_E}{r^2}\left\{\cos\gamma\left[-1 + \frac{9}{2}J_2\left(\frac{R_E}{r}\right)^2\left(\cos^2\theta - \frac{1}{3}\right)\right] + \sin\gamma\cos\xi\left[\frac{3}{2}J_2\left(\frac{R_E}{r}\right)^2\sin(2\theta)\right]\right\}\right) + \frac{V\cos\gamma}{r} \tag{2b}$$

$$\dot{\xi} = \left(\frac{1}{V\cos\gamma}\right)\left(-\frac{1}{2}\rho(r - R_E)V^2(x_9 + w_3) + \frac{\mu_E}{r^2}\left\{\sin\xi\left[\frac{3}{2}J_2\left(\frac{R_E}{r}\right)^2\sin(2\theta)\right]\right\}\right) + \frac{V\cos\gamma\sin\xi\cos\theta}{r\sin\theta} \tag{2c}$$

$$\dot{r} = V\sin\gamma \tag{2d}$$

$$\dot{\theta} = -\frac{V\cos\gamma\cos\xi}{r} \tag{2e}$$

$$\dot{\phi} = -\frac{V\cos\gamma\sin\xi}{r\sin\theta} - \omega_E \tag{2f}$$

$$\dot{x}_7 = w_4 \tag{2g}$$

$$\dot{x}_8 = w_5 \tag{2h}$$

$$\dot{x}_9 = w_6 \tag{2i}$$

where the function $\rho(r - R_E)$ is the standard atmospheric density as a function of altitude,[5] R_E is the mean Earth radius, μ_E is the geocentric gravitational constant, J_2 is a constant of the Earth's gravitational field, ω_E is the Earth's rotation rate, and w_1–w_6 are the elements of the modeled random disturbance effects. These random disturbances are modeled as Gaussian white noise. The quantities x_7, x_8, and x_9 correspond to SC_L/m, SC_D/m, and SC_Y/m, respectively. All angles are in radians, and all other units are in the mks system. These equations are in the general form

$$\dot{x} = f(x, w) \tag{3}$$

where the elements of the nonlinear vector function $f(x, w)$ are defined by the right-hand sides of Eqs. (2).

Filter Measurement Model

The magnitude of the Earth's magnetic field vector at the spacecraft is the measured quantity that provides corrections to the state vector. This quantity gets computed in two ways, one based on the actual magnetometer measurements and the other based on an a priori state estimate. The magnitude based on measurements is

$$y = \sqrt{B_x^2 + B_y^2 + B_z^2} \tag{4}$$

where B_x, B_y, and B_z are the readings on the three axes of the onboard magnetometer. The magnitude based on the state estimate is

$$h(x) = \sqrt{B_r^2(r, \theta, \phi) + B_\theta^2(r, \theta, \phi) + B_\phi^2(r, \theta, \phi)} \tag{5}$$

where the functions $B_r(r, \theta, \phi)$, $B_\theta(r, \theta, \phi)$, and $B_\phi(r, \theta, \phi)$ are the zenith, south, and east components of the Earth's magnetic field vector at location (r, θ, ϕ). These functions are defined by a spherical harmonic expansion whose coefficients are based on curve fitting of Earth-based and satellite-based magnetic observatory data.[6] The coefficients that have been used are those of the 10th-order IGRF 1980 and 1985 models with propagation of secular effects out to the eighth-order terms. These models can be found in Ref. 6, pp. 348 and 349.

The derivative of $h(x)$ with respect to x is needed to do extended Kalman filtering. This creates the need to take derivatives of the functions $B_r(r, \theta, \phi)$, $B_\theta(r, \theta, \phi)$, and $B_\phi(r, \theta, \phi)$ with respect to r, θ, and ϕ. These derivatives are determined analytically in the filters reported in this paper. The details of the necessary differentiations are too numerous to report here, but two important points, which make the derivative computations more efficient, will be discussed.

The field vector, $(B_r, B_\theta, B_\phi)^T$, is the gradient of a scalar potential function. Therefore, the following three relationships hold among their first derivatives:

$$\frac{\partial B_r}{\partial\theta} = r\frac{\partial B_\theta}{\partial r} + B_\theta \tag{6a}$$

$$\frac{\partial B_r}{\partial\phi} = \left(r\frac{\partial B_\phi}{\partial r} + B_\phi\right)\sin\theta \tag{6b}$$

$$\frac{\partial B_\theta}{\partial\phi} = \sin\theta\frac{\partial B_\phi}{\partial\theta} + \cos\theta\, B_\phi \tag{6c}$$

These three relationships follow directly from the symmetry of the scalar potential function's second derivative matrix. These

relations can be used to reduce the required number of first derivative calculations from nine to six.

Evaluation of the B_r, B_θ, and B_ϕ functions can be done efficiently via a recursive algorithm that computes the necessary Legendre functions.[6] Efficient derivative calculation can be achieved via differentiation of the entire recursive algorithm. Also, differentiation of the factors that depend on ϕ yields other factors that are already part of the computation.

Square Root Information Filter Implementation

The SRIF is a special form of the Kalman filter that calculates and stores the state estimate and covariance in a numerically stable way. This section extends the SRIF to work with nonlinear plant dynamics and measurement equations. The SRIF for linear systems is well documented in Bierman,[7] and the following discussion of the nonlinear SRIF assumes that the reader is familiar with Ref. 7. Instead of a state estimate and a state covariance matrix, the SRIF operates on a state information equation:

$$\boldsymbol{R}_k \boldsymbol{x}_k = z_k + \nu_k \tag{7}$$

This equation implicitly determines the state vector $\boldsymbol{x}_k$ in terms of the known matrix $\boldsymbol{R}_k$, the known vector z_k, and the uncertain vector ν_k. The latter vector is a Gaussian, zero-mean, unit variance, uncorrelated random vector: $E[\nu_k] = \mathbf{0}$ and $E[\nu_k \nu_j^T] = \boldsymbol{I}\delta_{k,j}$. The state estimate is $\hat{\boldsymbol{x}}_k = E[\boldsymbol{x}_k] = \boldsymbol{R}_k^{-1} z_k$, and the covariance is $E[(\boldsymbol{x}_k - \hat{\boldsymbol{x}}_k)(\boldsymbol{x}_k - \hat{\boldsymbol{x}}_k)^T] = \boldsymbol{R}_k^{-1}\boldsymbol{R}_k^{-T}$. These formulas can be derived by solving Eq. (7) for $\boldsymbol{x}_k$ in terms of $\boldsymbol{R}_k$, z_k, and ν_k and taking the required expectations.

Propagation of the state information equation from time t_k to time t_{k+1} is performed using the nonlinear filter equations of motion. [The following procedure is an adaptation of the extended Kalman filter (EKF) technique to the SRIF data structure.] Suppose $\hat{\boldsymbol{x}}_k$ is the a posteriori state estimate at sample time t_k. Also, suppose that the statistics of $\boldsymbol{w}_k$, a discrete-time white noise disturbance vector, are defined by an information equation:

$$\boldsymbol{R}_{w_k} \boldsymbol{w}_k = z_{w_k} \nu_{w_k} \tag{8}$$

where ν_{w_k} is a random vector with statistics similar to ν_k (Gaussian, zero-mean, unit variance, uncorrelated for different k). The matrix $\boldsymbol{R}_{w_k}$ and the vector z_{w_k} effectively store the mean and the covariance of $\boldsymbol{w}_k$: $\hat{\boldsymbol{w}}_k = E[\boldsymbol{w}_k] = \boldsymbol{R}_{w_k}^{-1} z_{w_k}$, and $E[(\boldsymbol{w}_k - \hat{\boldsymbol{w}}_k)(\boldsymbol{w}_k - \hat{\boldsymbol{w}}_k)^T] = \boldsymbol{R}_{w_k}^{-1}\boldsymbol{R}_{w_k}^{-T}$. One can propagate the dynamic model as in an extended Kalman filter: solve the following initial value problem for $\mathbf{x}(t)$.

$$\dot{\mathbf{x}} = \boldsymbol{f}(\mathbf{x}, \hat{\boldsymbol{w}}_k) \tag{9a}$$

subject to

$$\mathbf{x}(t_k) = \hat{\boldsymbol{x}}_k \tag{9b}$$

Given this solution, one can then derive a linearized state difference equation:

$$\boldsymbol{x}_{k+1} - \mathbf{x}(t_{k+1}) = \Phi_k[\boldsymbol{x}_k - \hat{\boldsymbol{x}}_k] + \Gamma_k[\boldsymbol{w}_k - \hat{\boldsymbol{w}}_k] \tag{10}$$

where the state transition matrix Φ_k and the disturbance effectiveness matrix Γ_k are computed using linearizations of Eqs. (9) about $\mathbf{x}(t)$ and $\hat{\boldsymbol{w}}_k$. Solution of Eq. (10) for $\boldsymbol{x}_k$ and substitution of the result into Eq. (7), the information equation at sample k, yields an equation in the unknowns $\boldsymbol{w}_k$ and $\boldsymbol{x}_{k+1}$:

$$[-\boldsymbol{R}_k \Phi_k^{-1}\Gamma_k]\boldsymbol{w}_k + [\boldsymbol{R}_k \Phi_k^{-1}]\boldsymbol{x}_{k+1} = \left(z_k - \boldsymbol{R}_k\{\hat{\boldsymbol{x}}_k + \Phi_k^{-1}[\Gamma_k \hat{\boldsymbol{w}}_k - \mathbf{x}(t_{k+1})]\}\right) + \nu_k \tag{11}$$

Bierman[7] gives the details of how to combine Eqs. (8) and (11) via left orthogonal/upper triangle (QR) factorization to eliminate $\boldsymbol{w}_k$ and get an a priori state information equation at sample instant t_{k+1} of the form:

$$\boldsymbol{R}_{k+1}^{-}\boldsymbol{x}_{k+1} = z_{k+1}^{-} + \nu_{k+1}^{-} \tag{12}$$

which completes the propagation of the information equation.

For long intervals between measurement updates, multiple iterations of Eqs. (7–12) must be used to propagate the state information equation. Each iteration propagates the equation over a portion of the interval, and Eq. (12) at the end of a given subinterval serves the function of Eq. (7) at the beginning of the next subinterval. This subdivision of long intervals is necessary to adequately approximate the continuous-time white-noise disturbance process in Eqs. (2) and (3) by the discrete-time white noise sequence $\boldsymbol{w}_k, \boldsymbol{w}_{k+1}, \ldots$.

Extension of the SRIF measurement update to the nonlinear problem begins by adding a measurement noise, n_{k+1} ($E[n_{k+1}] = 0$, $E[n_{k+1}n_j] = \sigma^2\delta_{k+1,j}$), to the nonlinear measurement model to explain any difference between the sensed value of a quantity, Eq. (4), and the corresponding estimated value, Eq. (5):

$$y_{k+1} = h(\boldsymbol{x}_{k+1}) + n_{k+1} \tag{13}$$

The SRIF needs to work with a linear approximation of this equation that has been transformed into the standard measurement information equation form of Ref. 7:

$$\boldsymbol{A}_{m_{k+1}}\boldsymbol{x}_{k+1} = z_{m_{k+1}} + \nu_{m_{k+1}} \tag{14}$$

where $\boldsymbol{A}_{m_{k+1}}$ is called the measurement information matrix, $z_{m_{k+1}}$ is called the measurement information vector, and the vector $\nu_{m_{k+1}}$ is a Gaussian, zero-mean, unit variance, uncorrelated random vector. Equation (13) can be put into the form of Eq. (14). First, linearize it about $\mathbf{x}(t_{k+1})$, the a priori state estimate at time t_{k+1}. After rearrangement of terms and multiplication by $1/\sigma_{k+1}$, the linearized equation becomes

$$\left[\frac{1}{\sigma_{k+1}}\frac{\partial h}{\partial \boldsymbol{x}}\bigg|_{\mathbf{x}(t_{k+1})}\right]\boldsymbol{x}_{k+1} = \left(\frac{1}{\sigma_{k+1}}\{y_{k+1} - h[\mathbf{x}(t_{k+1})] + \left[\frac{\partial h}{\partial \boldsymbol{x}}\bigg|_{\mathbf{x}(t_{k+1})}\right]\mathbf{x}(t_{k+1})\}\right) + \nu_{m_{k+1}} \tag{15}$$

where $\nu_{m_{k+1}} = -n_{k+1}/\sigma_{k+1}$. The matrix $\boldsymbol{A}_{m_{k+1}}$ and the vector $z_{m_{k+1}}$ in Eq. (14) correspond to the two expressions in large brackets or parentheses in Eq. (15). Bierman[7] describes how to compute the SRIF measurement update by combining Eqs. (12) and (14) via left QR factorization to yield an a posteriori information equation at sample $k+1$ of the form:

$$\boldsymbol{R}_{k+1}\boldsymbol{x}_{k+1} = z_{k+1} + \nu_{k+1} \tag{16}$$

This last operation is closely related to a least-squares solution of an overdetermined system of equations. As stated earlier, this measurement information equation implicitly defines the a posteriori state estimate and covariance.

Statistical Modeling of Noise and Disturbances

The statistical model of the measurement noise is the model of the random scalars $n_k, n_{k+1}, n_{k+2}, \ldots$. They have been modeled as a zero mean, uncorrelated Gaussian sequence of numbers with an altitude dependent variance, $\sigma_{k+1} = \sigma_{k+1}(r_{k+1})$. The dependence of variance on radial distance from the center of the Earth is taken from Ref. 5 (p. 118). Essentially, this noise model assumes that the main error contribution is from uncertainty in the IGRF model of the Earth's magnetic field. This uncertainty decays with increasing altitude. For low-Earth orbits, the magnitude of the field model uncertainty is large enough to make this statistical model acceptable even when random magnetometer error contributions are appreciable.

If magnetometer biases are present, then this model breaks down, but the way to deal with biases is to estimate them rather than to amend the measurement noise model. This is done for the batch filter.

The plant disturbance model gives the statistics of the $\boldsymbol{w}_k$ vectors. Equation (8) constitutes this model. The principal disturbances to low-Earth orbits are aerodynamic. The disturbances w_1-w_3 are partially nondimensionalized aerodynamic disturbance forces. They have the units of inverse ballistic coefficients, m^2/kg. The disturbances w_4-w_6 are rates of change of random-walk aerodynamic disturbance forces. All of these quantities are assumed to have zero mean (the nonzero steady drag force will be estimated by x_8). Therefore, $z_{w_k} = \mathbf{0}$. Because of their partial nondimensionalizations, the variances of the disturbances w_1-w_3 can be sized based on typical fractional variations of the atmospheric density divided by a typical ballistic coefficient. These variances have been chosen to be 2.5×10^{-3} m^2/kg. The w_4-w_6 variances have been set at $(0.04\ m^2/kg)/T$, where T is the estimated orbital period. For low-Earth orbit, these variances are about 7×10^{-6} $m^2/(kg\text{-}s)$. The offdiagonal elements of $\boldsymbol{R}_{w_k}$ have each been set to zero, and the diagonal elements have each been set to the inverse of the variance of the corresponding w element.

B. Batch Least-Squares Filter

Estimation Parameter Vector

A batch filter has been used to estimate the spacecraft orbit in terms of Keplerian-type elements. Additionally, magnetometer biases have been included in the estimation vector. This static vector of parameters has 10 elements:

$$\boldsymbol{p} = [M_0, M_1, M_2, e, \omega_0, \lambda_0, i, b_x, b_y, b_z]^T \tag{17}$$

where the first seven elements define the estimated orbit and the last three elements are magnetometer biases in the spacecraft coordinate system.

The orbit parameters consist of six typical Keplerian elements plus an ad hoc decay coefficient that has been used by the Naval Research Laboratory.[8] The orbit parameters' definitions are

M_0 = mean anomaly at epoch, rad
M_1 = mean motion, rad/s
M_2 = decay coefficient, rad/s^2
e = eccentricity
ω_0 = argument of perigee at epoch, rad
λ_0 = longitude of the ascending node at epoch, rad
i = inclination, rad

Position Calculation

The first seven parameters of the $\boldsymbol{p}$ vector, along with the time since epoch, Δt (s), serve to define the spacecraft position. The following calculations account for mean J_2 effects and orbit decay. The mean J_2 corrections reported here are correct to first order in J_2 and can be derived from equations appearing in Ref. 9. The position determination begins with the calculation of the mean semimajor axis $\bar{a}$:

$$a_M = [806.81359\, M_1]^{-2/3} \tag{18}$$

$$a_0 = a_M \left[1 + \frac{0.75 J_2 (3 \cos^2 i - 1)}{a_M^2 (1 - e^2)^{3/2}} \right]^{-2/3} \tag{19}$$

$$\bar{a} = a_0 \left[1 - \frac{0.75 J_2 (3 \cos^2 i - 1)}{a_M^2 (1 - e^2)^{3/2}} \right] \tag{20}$$

The quantities a_M and a_0 are intermediate results. The quantities a_M, a_0, and $\bar{a}$ are in units of Earth radii. The uncorrected mean semimajor axis a_0 is used in calculations of the mean J_2-induced precession rates of the perigee and the line of nodes:

$$\omega' = \frac{0.75 J_2 (5 \cos^2 i - 1)}{a_0^2 (1 - e^2)^2} \tag{21}$$

$$\Omega' = \frac{-1.5 J_2 \cos i}{a_0^2 (1 - e^2)^2} \tag{22}$$

where both precession rates are in units of radians per radian of mean motion. The rate of decay of the mean semimajor axis is modeled as

$$\dot{a} = -(4/3)\bar{a}(M_2/M_1) \tag{23}$$

The next steps in the position calculation propagate various quantities to the time past epoch Δt. They are the mean anomaly, the argument of perigee, the longitude of the ascending node, and the semimajor axis:

$$M = M_0 + M_1 \Delta t + M_2 \Delta t^2 \tag{24a}$$

$$\omega = \omega_0 + \omega' [M_1 \Delta t + M_2 \Delta t^2] \tag{24b}$$

$$\lambda = \lambda_0 + \Omega' [M_1 \Delta t + M_2 \Delta t^2] \tag{24c}$$

$$a = \bar{a} + \dot{a} \Delta t \tag{24d}$$

To get the true anomaly v, the eccentric anomaly E is first determined via a Newton-Raphson numerical solution of Kepler's equation:

$$M - E + e \sin(E) = 0 \tag{25}$$

The true anomaly can then be computed:

$$v = \tan^{-1} \left[\frac{\sqrt{1 - e^2} \sin E}{\cos E - e} \right] \tag{26}$$

Finally, the "mean" spacecraft position can be computed in terms of radial distance from the Earth's center, colatitude, and east longitude:

$$r = R_E\, a (1 - e \cos E) \tag{27a}$$

$$\theta = \cos^{-1} [\sin (\omega + v) \sin i] \tag{27b}$$

$$\phi = \tan^{-1} \left[\frac{\sin \lambda \cos(\omega + v) + \cos \lambda \sin(\omega + v) \cos i}{\cos \lambda \cos(\omega + v) - \sin \lambda \sin(\omega + v) \cos i} \right] \tag{27c}$$

The batch filter also needs the derivatives of r, θ, and ϕ with respect to the elements of $\boldsymbol{p}$. Of course, the only nonzero derivatives are those with respect to the first seven elements of $\boldsymbol{p}$. The filter uses analytic derivatives of these quantities, which are calculated via differentiation of Eqs. (18–27).

Measurement Model

The measurement model is similar to that of the SRIF extended Kalman filter. The modeled magnetic field magnitude at sample instant k is a function of time since epoch and the first seven elements of $\boldsymbol{p}$:

$$\begin{aligned} h(\boldsymbol{p}, \Delta t_k) = \{ & B_r^2 [r(\boldsymbol{p}, \Delta t_k), \theta(\boldsymbol{p}, \Delta t_k), \phi(\boldsymbol{p}, \Delta t_k)] \\ & + B_\theta^2 [r(\boldsymbol{p}, \Delta t_k), \theta(\boldsymbol{p}, \Delta t_k), \phi(\boldsymbol{p}, \Delta t_k)] \\ & + B_\phi^2 [r(\boldsymbol{p}, \Delta t_k), \theta(\boldsymbol{p}, \Delta t_k), \phi(\boldsymbol{p}, \Delta t_k)] \}^{1/2} \end{aligned} \tag{28}$$

This equation is similar to Eq. (5). The only difference is that r, θ, and ϕ are explicitly estimated in the sequential filter

associated with Eq. (5), whereas, in Eq. (28), the position is inferred from the estimates of the seven orbit parameters.

The measured magnetic field gets altered before use in the batch least-squares calculation. Instead of Eq. (4), the following model is used:

$$y_k(\boldsymbol{p}) = \sqrt{[B_{x_k} - b_x]^2 + [B_{y_k} - b_y]^2 + [B_{z_k} - b_z]^2} \qquad (29)$$

where B_{x_k}, B_{y_k}, and B_{z_k} are the readings on the three axes of the onboard magnetometer at sample k. Equation (29) removes the estimated biases from the measured field vector before computing the measured field magnitude. Therefore, the "measurement" is a function of $\boldsymbol{p}$.

Statistical Model and Least-Squares Cost Function

The least-squares cost function minimizes the mean square error between the measured field magnitudes and the modeled field magnitudes. The batch filter assumes that the difference between these two quantities is due to a measurement error n_k:

$$y_k(\boldsymbol{p}) = h(\boldsymbol{p}, \Delta t_k) + n_k \qquad (30)$$

for all samples $k = 1, 2, \ldots, N$. It also assumes that the sequence $n_1, n_2, n_3, \ldots, n_N$ is random, Gaussian, zero mean, and uncorrelated with a variance of $\sigma = 270$ nT. The least-squares cost function is then expressed as the negative of the likelihood:

$$J(\boldsymbol{p}) = \frac{1}{2\sigma^2} \sum_{k=1}^{N} [y_k(\boldsymbol{p}) - h(\boldsymbol{p}, \Delta t_k)]^2 \qquad (31)$$

The reason for expressing the cost as a negative likelihood is to facilitate statistical analysis of the quality of the answer. After minimization of J, the covariance of the minimizing $\boldsymbol{p}$ vector is approximately the inverse of the Hessian of this negative likelihood function.

Minimization Algorithm

The Gauss-Newton method for least-squares problems has been used by the batch filter. It is a gradient-based search algorithm that takes advantage of the special least-squares structure.[10] It computes a search direction by linearizing Eq. (30) about a guessed $\boldsymbol{p}$ and solving a least-squares problem for the resulting overdetermined linear system. This is done using left QR factorization. The resulting search direction is guaranteed to be a descent direction for the original nonlinear least-squares cost function, Eq. (31). The search step length is determined by a one-dimensional minimization subject to a maximum step length constraint. If the optimal cost is near zero, the Gauss-Newton method will have a near quadratic rate of convergence. Search direction computation is quick; it requires only first derivatives, all of which are computed analytically.

III. Spacecraft Test Cases

A. MAGSAT Spacecraft

The mission of the Magnetic Field Satellite (MAGSAT)[11] was to do a global magnetic survey. It was launched in October 1979 into a near polar low-Earth orbit. Its orbital characteristics on February 2, 1980, were 97-deg inclination, 0.0125 eccentricity, 330-km perigee height, and 500-km apogee height.

The spacecraft had two magnetometers: a scalar cesium vapor magnetometer and a vector fluxgate magnetometer. The scalar magnetometer was used by NASA to calibrate the vector magnetometer. Both were mounted on a 6-m boom to reduce stray fields from the spacecraft to less than 1 nT. The precision of the vector magnetometer was better than 1 nT and its accuracy was better than 6 nT rms over a measurement range of $\pm 64{,}000$ nT.

Reference 11 describes MAGSAT data that are available on computer tapes. This project used Investigator B quiet time data from February 2, 1980. The quiet time data were taken during times of low solar magnetic storm activity. The tape data include geocentric radius, latitude, longitude, magnetic field magnitude (vector magnetometer), and 5-s averages of magnetic field magnitude (vector magnetometer), with each piece of data available at 5-s intervals. The tape's magnetic field magnitude and averaged magnetic field magnitude both have been used to estimate spacecraft position using the filters of this paper. These estimates, in turn, have been compared with the position data on the MAGSAT tape, which are accurate to within 0.5 km.

The MAGSAT data represent a best case for the algorithms of this paper for two reasons. First, the magnetic field measurements were very accurate; the accuracy of the magnetometer was very high, and it was located far away from sources of spacecraft-generated fields. Second, the field model used by the filters for this case, the 1980 IGRF model, is largely based on MAGSAT data. Therefore, it is a reliable model for the time period and location of the data being filtered.

The use of 1980 IGRF data to filter MAGSAT data is, in a sense, circular reasoning. MAGSAT's location had to be known from tracking data to generate the field model. The field model, in turn, has to be known to filter for position. Nevertheless, this test case can demonstrate three key points: the mathematical observability of orbits from magnetometer data alone, the ability to estimate position in the face of actual disturbance forces, and the ability to estimate position in the face of random measurement/modeling errors on the order of 30–90 nT rms (typical filter residual errors achieved in this study).

B. DE-2 Spacecraft

The Dynamics Explorer-2 (DE-2) spacecraft was launched to study the flow of solar energy and matter from space through the Earth's magnetic field into the upper atmosphere. It was launched in August 1981 into an elliptical polar orbit. During March 1982 its orbital characteristics were 90-deg inclination, 0.038 eccentricity, 290-km perigee height, and 810-km apogee height.

DE-2's mission required that it have an accurate magnetometer. The spacecraft had a vector magnetometer. It had biases on the order of 1 nT per axis. Spacecraft-generated fields were less than 10 nT. The position of DE-2 has been tracked from the ground to within 1 km. The tracking data provide the truth model for evaluating the performance of the MAGNAV filter.

The filtered DE-2 magnetometer data have been specially chosen to fall during magnetically quiet times (when no solar magnetic storms were occurring). Data are not continuously available for the DE-2 spacecraft because it did not have a 100% duty cycle of telemetry recording. When data are available, they occur at 60-s intervals but are grouped in batches that last anywhere from 15 min to 2 h. Intervals of data unavailability last as long as 6 h during the two 2-day periods for which the filter has been tested.

The DE-2 data represent an intermediate level of difficulty for the navigation technique of this paper. The accurate field measurements and low spacecraft-generated fields onboard DE-2 improve the expected accuracy of the technique. On the other hand, the reduced accuracy of the 1980 IGRF field model, when propagated to 1982 using secular terms, would tend to degrade the MAGNAV technique's accuracy. This test case avoids the circular reasoning of the MAGSAT case; therefore, it tests the orbit determination concept under typically expected uncertainties about the Earth's magnetic field model.

C. LACE Spacecraft

The Low-Power Atmospheric Compensation Experiment (LACE) spacecraft was launched in February 1990 into an inclined low-Earth orbit. Its orbital characteristics on June 3,

1990, were 43-deg inclination, 0.0016 eccentricity, 524-km perigee height, and 546-km apogee height.

The spacecraft had one vector fluxgate magnetometer. The magnetometer's purpose was to do backup attitude determination.[12] Its accuracy was specified to be 500 nT per channel, which included possible biases of 300 nT per channel. Ground tests indicated that its actual accuracy, excluding biases, was probably 120 nT or better. It was mounted inside the main spacecraft module just behind a solar panel. Ground tests indicated that the solar panel could produce a field of 156 nT at the magnetometer. Ground testing for additional spacecraft-generated fields was not done.

Data from June 6, 1990, have been used to test the batch filter. It is available at 100-s intervals. The spacecraft ephemeris has been determined from tracking stations. It is supplied in terms of the seven orbital elements described in Sec. II. B. The position estimated by the filter has been compared with this tracking-station-generated position. These elements give position to an accuracy of 4 km at epoch. The along-track accuracy deteriorates after epoch because of the large variability of the drag. A timing bias uncertainty in the LACE magnetometer data set further degrades the accuracy of the along-track truth model. For the case considered in this paper, the along-track position derived from tracking data could have an error as large as 80 km. Any such error would be roughly constant during a day's worth of filtering. The cross-track and radial errors in the tracking data are no more than 4 km.

The LACE spacecraft represents a difficult case for magnetometer-based navigation in low-Earth orbit. First, sizable systematic errors are caused by solar-array-generated time-varying fields. Second, the IGRF 1985 field model has been used with secular propagation of coefficients to 1990. Because of this long secular propagation (extrapolation), the accuracy of this field model is probably lower than the accuracies of the field models used for the MAGSAT and DE-2 studies.

IV. Filter Performance Evaluation Methods

Several criteria have been used to evaluate filter performance for accuracy and practicality. The accuracy has been evaluated by comparing the estimated spacecraft position with the position supplied by ground-station tracking. Total position error, component errors (along-track error, cross-track error, and altitude error), and rms error have all been computed.

In addition to actual accuracy, predicted accuracy has also been evaluated. Each of the two filters of Sec. II incorporates a statistical model of measurement errors. The SRIF also has a statistical model of disturbances. These statistical models can be used to compute a modeled position error covariance. In the case of the square root information filter (Sec. II. A), the position covariance is directly available as a submatrix of the total filter covariance, $\boldsymbol{R}_k^{-1}\boldsymbol{R}_k^{-T}$. In the case of the batch filter (Sec. II. B), the position covariance can be inferred from the parameter vector's covariance. This is done via a linear analysis involving the derivative of the position with respect to the seven orbit parameters. Although the parameters are static, the position derivatives depend on time since epoch. Therefore, the position covariance varies with time since epoch.

Computation of the modeled covariance reveals several filter characteristics. First, the modeled covariance demonstrates observability. In the SRIF case, convergence of the position covariance to small values implies observability. In the batch filter case, a low overall position covariance shows batch observability, which is another way of saying that the minimum of the batch least-squares problem is sufficiently well defined. Position covariances indicate the expected effects of the modeled random processes on filter accuracy. Deviation of the actual accuracy from the predicted accuracy would indicate one of two things: mismodeled statistics of the random processes or the presence of systematic errors.

The practicality of autonomous implementations of the filters depends on their computation time and RAM space requirements. These will also be evaluated for the cases considered next.

V. MAGSAT Performance

Both filters, the SRIF and the batch filter, have been tested with MAGSAT data. Both have filtered data that were taken on or about February 2, 1980. The SRIF position/velocity determination system could be used because MAGSAT's magnetometer biases were negligible. Although not needed for this good data set, the batch filter also was tried to test its functioning and to compare its performance with the SRIF.

A. SRIF Results

The SRIF filter has been tried with a variety of initial errors and two different sample intervals. Both raw magnitude data and 5-s averaged magnitude data have been used. Figure 1 shows the total position error time history for one of these cases. The sample interval is 25 s, the initial velocity error magnitude is 1000 m/s, and the initial position vector error magnitude is 1000 km. Averaged magnitude data have been used. Figure 2 shows the corresponding along-track error, and Fig. 3 shows the cross-track error. This performance is encouraging; the total position error decreases from 1000 km to less then 8 km in less than one day. This convergence indicates observability of the orbit from magnetometer measurements alone. Most of the errors after 24 h are in the horizontal plane. Figure 2 shows a slowly varying along-track error. The peri-

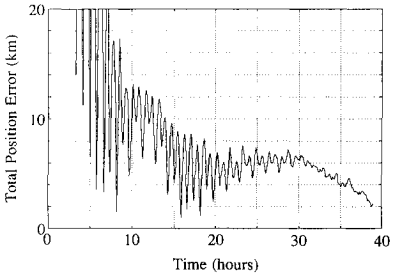

Fig. 1 Total position error vs time for the SRIF operating on MAGSAT data.

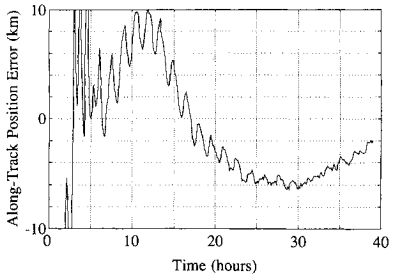

Fig. 2 Along-track position error vs time for the SRIF operating on MAGSAT data.

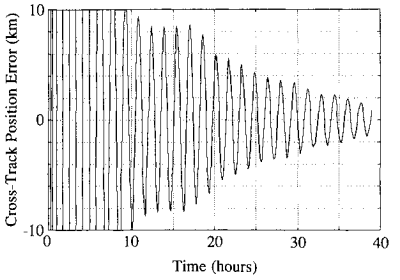

Fig. 3 Cross-track position error vs time for the SRIF operating on MAGSAT data.

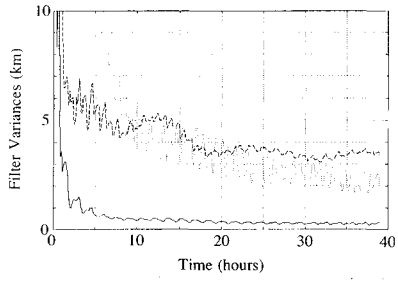

Fig. 4 SRIF modeled position variances for MAGSAT case (dotted line: along track; dashed line: cross track; solid line: altitude).

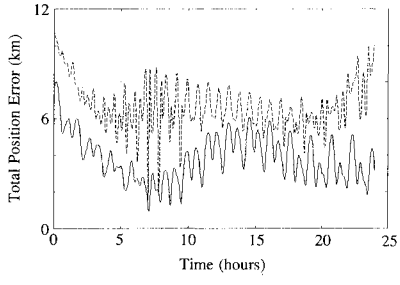

Fig. 5 Total position error and associated variance vs time for the batch filter operating on MAGSAT data (solid line: actual error; dashed line: filter's modeled variance).

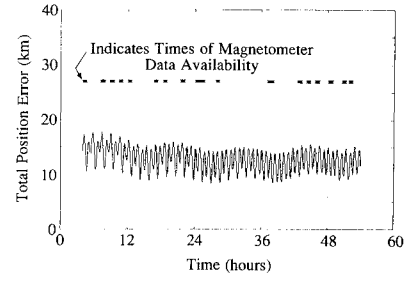

Fig. 6 Total position error vs time for the batch filter operating on DE-2 data.

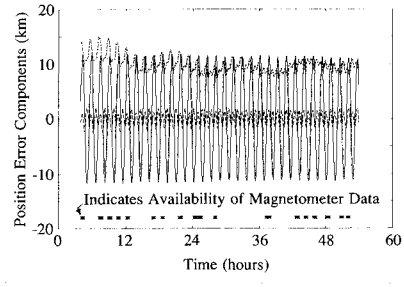

Fig. 7 Three position error components vs time for the batch filter operating on DE-2 data (dash-dot line: along track; sold line: cross track; dashed line: altitude).

odic cross-track error of Fig. 3 implies some inaccuracy of the filter's determination of the orbital plane. The altitude error, not shown, remains less than 1 km after 20 h of filtering.

The filter's estimated position variances are plotted in Fig. 4. This corresponds to the same case as Figs. 1–3. The dotted line is the along-track variance, the dashed line is the cross-track variance, and the solid line is the altitude variance. These variances all decrease from larger initial values, which implies observability of the system. The variances after 24 h of filtering are comparable to the actual errors. This indicates that the filter's statistical model is probably reasonable.

A number of other runs of the SRIF have been performed on the same set of MAGSAT data. A two-iteration measurement update has been tried in an attempt to reduce the effects of measurement equation nonlinearities. This technique iterates Eqs. (14–16) twice. It reduces the total error to 4 km in some cases. Different initial conditions sometimes produce filter divergence or slowed convergence, but convergence as in Figs. 1–3 seems to be guaranteed if the initial velocity error's magnitude is less than 300 m/s and if the initial position error's magnitude is less than 300 km. A long interval of data unavailability (3 h) does not cause problems if the information equation gets propagated via multiple 100-s steps of Eqs. (7–12) and if a two-iteration measurement update gets used. Changes of the modeled noise and disturbance variances by a factor of two do not significantly affect results. When the normal single-iteration measurement update is used, a lengthened sample interval (sample period = 100 s) sometimes produces much poorer accuracy, depending on the initial estimation error.

The SRIF computations have been done on an 80286-based microcomputer running at 6 MHz and using a math coprocessor. The filter requires 78 kilobytes of RAM. It takes 3.65 s of execution time per measurement sample. This translates into 15% of a comparable flight computer's time if a sample period of 25 s is used.

B. Batch Filter Results

The batch filter has achieved accuracies comparable to that of the SRIF. A case has been run that uses 24 h worth of data sampled at 100-s intervals. Raw magnetometer data have been used in this case (as opposed to 5-s averaged data).

The total position error for this case is shown in Fig. 5, the solid line. The covariance for this case has also been computed. At any given time, the covariance matrix and the actual error direction can be used to compute the variance along the direction of the actual error. This variance is plotted as the dashed line of Fig. 5. The actual error is less than 8 km, and its rms value is 4 km. The predicted variance is somewhat higher.

The three components of the position error have been computed and compared with the filter's predicted variances. Although not shown on a figure, the along-track error is 3.4-km rms, and the predicted along-track variance stays between 5 and 11 km; recall that the filter's predicted variance is a function of time. The cross-track error is a steady once-per-orbit oscillation with an rms value of 1.8 km, and the predicted cross-track variance oscillates between 6.5 and 10 km. The altitude error is a steady twice-per-orbit oscillation with an rms value of 1.2 km, and the predicted altitude variance is steady at 1 km. The actual errors and the modeled statistics seem to be in rough agreement: in some cases the actual errors are slightly smaller than those predicted by the filter, whereas they are slightly larger than the predicted errors in other cases. In any case, the achieved accuracy of less than 10-km peak error is significant.

The batch filter computations also have been done on a 6-MHz 80286-based microcomputer with a math coprocessor. The filter requires 300 kilobytes of RAM to handle 1000 data points using double precision arithmetic. The filter memory requirement is dependent on the number of samples that it can handle. For a case when an extremely poor first guess was used (the guessed initial orbit parameters yielded a 3200-km rms position error over one day), the execution time was 10.5 h (86 Gauss-Newton iterations) to solve for the orbit. This slow convergence was caused in part by the algorithm's limit on step length. Even so, this would be only 44% of flight computer time, and such drastic adjustments in the orbital estimate would probably be needed only infrequently, perhaps only immediately after launch, if ever. Typical daily adjustments to the orbit estimate might require eight iterations or fewer, using up only 1 hour (4% of flight computer time). Execution times reported here are for 853 samples. Execution time varies linearly with changes in the number of samples being processed.

VI. DE-2 Performance

The batch filter has been further tested using data from the DE-2 spacecraft. The SRIF was not tested on the DE-2 data because it might have difficulties dealing with the frequent long gaps in the DE-2 magnetometer data set.

One filter test case has used data spread over the time frame of March 15–17, 1982. Figure 6 plots the total position error vs time for this case. The x marks on the figure indicate the times at which magnetometer data is available (the same holds true for the x marks on Fig. 7). Figure 7 gives the three components of the position error, along track (dash-dot curve, positive when the estimated position is ahead of the actual position), cross track (solid curve, positive when the estimated position is right of the actual position), and altitude (dashed curve, positive when the estimated position is below the actual position). The altitude curve is difficult to see because of overlap with the cross-track curve. It oscillates between -2 and $+2$ km.

Figure 7 indicates that the worst-case error component is the along-track error, which hovers between 8 and 15 km. The cross track oscillates at the orbital period with a constant amplitude during the entire run, and the altitude error oscillates at twice the orbital period with a constant amplitude. The along-track error has a small oscillatory component combined with a slow drift. This drift is due to inaccuracy in the estimation of the mean motion and the decay coefficient. Modeled variance calculations indicate that the actual cross-track accuracy is somewhat better than that predicted by the filter variance, whereas the actual along-track and altitude accuracies are on the order of the filter's predictions. The reason for the higher cross-track accuracy is unknown. The peak total position error for this case is 18 km (Fig. 6), which is a very respectable number for this unusual navigation filter.

Another interesting feature of Fig. 7 is the occurrence of oscillations in each error component. These are on the order of 5–24 km peak to peak. The batch filter includes the secular (long-term) effects of J_2, but it neglects the once-per-orbit short-term oscillatory effects, which can be on the order of 10 km (Ref. 9). This neglect of the short-term J_2 effects is one possible explanation for the error oscillations. The SRIF does not neglect these effects; therefore, it might not experience the same problems.

The batch filter estimates biases also. The bias component estimates for this case are -48.3, -7.3, and 35.3 nT. Their respective modeled variances are 29.0, 22.4, and 192.6 nT. The actual magnetometer biases for the DE-2 spacecraft are advertised as being on the order of 1 nT. The differences between the estimated biases and zero are all 1.7 standard deviations or less, which constitutes reasonable agreement with the advertised upper limit on biases. Furthermore, the low values of the filter's modeled bias estimation variances indicate that biases and orbit parameters are simultaneously observable.

An attempt has been made to improve performance of the batch filter by filtering data that are spread out over 12 days. This was done in hopes of getting improvements through the use of a larger data set. This did not work well because along-track error became large over such a long period. This happens because the batch filter's ephemeris routine is not accurate over long periods of time due to the ad hoc way in which it incorporates drag effects.

VII. LACE Performance

The batch filter also has been tested with LACE data. Biases on the LACE magnetometer could be significant (up to 300 nT according to specifications). Development of a bias estimation capability for the SRIF has not yet reached a stage of maturity. This is why SRIF results for the LACE spacecraft are not presented. Eighteen hours worth of data that were taken on or about June 6, 1990, have been filtered. The sample period is 100 s.

The batch filter's total error time history is plotted in Fig. 8 (solid curve). Also plotted is the filter's predicted variance in the direction of the total error vector (dashed curve). These curves are similar in nature to the curves plotted for the batch MAGSAT case in Fig. 5. The total position error is much larger than for MAGSAT or DE-2: the rms error is 88 km. The modeled variance is much lower than the actual error and is closer to the values found for the MAGSAT and DE-2 batch filter runs.

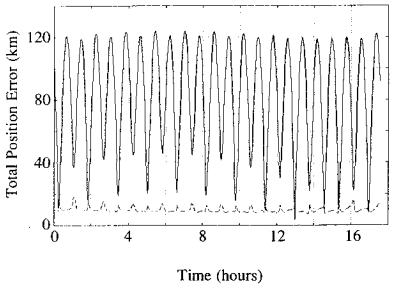

Fig. 8 Total position error and associated variance vs time for the batch filter operating on LACE data (solid line: actual error; dashed line: filter's modeled variance).

The large discrepancy between the true error statistics and the modeled statistics suggests the possibility of a systematic error. One possible source of observed error is not due to the magnetic orbit determination scheme at all; it is the large uncertainty in along-track truth model position noted in Sec. III. C. Better tracking data could reduce the along-track component of the observed error, but the largest error component, the across-track error, would remain (the rms altitude error is less than 6 km).

Another possible source of systematic error is the existence of slowly time-varying magnetic fields induced by the spacecraft at the magnetometer. Ground tests of the magnetometer with a solar array that is located near it showed that fields as large as 156 nT could be induced by the array. Tests for other sources of spacecraft noise were not performed.

If solar arrays produce significant magnetic fields at the magnetometer, they would probably produce fields that are periodic at the orbital frequency. This is because the spacecraft is Earth oriented via passive gravity-gradient stabilization. This periodic signal's magnitude and vector direction would vary slowly as the angle between the orbit normal and the sun vector changed due to precession. During a single day, however, the periodic term's magnitude and phase probably would be fairly constant.

Such periodic error terms are highly likely to degrade the filter's performance. An attempt has been made to estimate periodic error terms by augmenting the batch filter's estimation vector $\boldsymbol{p}$. Peak total navigation errors can be reduced from 125 to 85 km by such a scheme, which lends credence to the hypothesis that low-frequency solar-array-generated fields are responsible for the poor LACE performance. The augmented filter is impractical, however, because of poor observability of the augmented estimation vector.

Another source of systematic error could be the IGRF model of the Earth's magnetic field. The values used are 1985 values that have been propagated to 1990 using predicted secular terms. This is probably the main source of error for DE-2 cases where the overall errors are much smaller. The much smaller magnitudes of the DE-2 errors suggest that field model errors are not the principal cause of filter inaccuracy for the LACE case.

VIII. Conclusions

Two orbit determination filters have been described and tested. Both filters can autonomously determine orbit solely from magnetometer data. One is an extended square root information filter that estimates a position/velocity/distur-

bance-force state vector. The other is a batch least-squares filter that estimates Keplerian elements, a decay term, and biases.

Ground-based testing has been performed to evaluate these filters. Both filters have successfully converged from significant position and velocity errors. The batch least-squares filter has successfully estimated bias and orbit simultaneously. Using data from the Magnetic Field Satellite, both filters achieved positional accuracies between 4 and 8 km by filtering one day's worth of data. Batch filtering of two days' worth of data from the Dynamics Explorer-2 spacecraft yielded positional accuracies of 18 km or better. This decrease in accuracy for Dynamics Explorer-2 is probably due to the inaccuracy of the model used for the Earth's magnetic field. Batch filtering of the Low-Power Atmospheric Compensation Experiment spacecraft data yielded peak positional errors of 125 km. The very poor performance on this spacecraft may be due to slowly time-varying solar-array-induced fields.

The filters' performance on the Magnetic Field Satellite is probably a best-case scenario. Performance on the Low-Power Atmospheric Compensation Experiment spacecraft may be a worst-case scenario. Performance on the Dynamics Explorer-2 spacecraft may be typical of what can be achieved if an accurate magnetometer is used and if time-varying spacecraft-generated magnetic fields are kept low or are known and removed from the magnetometer signal.

Acknowledgments

Data from the MAGSAT spacecraft were provided by the National Space Science Data Center. Robert A. Langel was the principal investigator on the project that produced the MAGSAT data. Data from the DE-2 spacecraft were supplied by NASA Goddard Spaceflight Center with the help of James Byrnes and James Slaven. Data from the LACE spacecraft were supplied by the Naval Research Laboratory with the help of Michael Mook.

References

[1]Chory, M. A., Hoffman, D. D., and LeMay, J. L., "Satellite Autonomous Navigation—Status and History," *Proceedings of the IEEE Position, Location, and Navigation Symposium* (Las Vegas, NV), Inst. of Electrical and Electronics Engineers, New York, 1986, pp. 110–121.

[2]Tai, F., and Noerdlinger, P. D., "A Low Cost Autonomous Navigation System," *Guidance and Control 1989; Proceedings of the Annual Rocky Mountain Guidance and Control Conference* (Keystone, CO), American Astronautical Society, San Diego, CA, 1989, pp. 3–23 (AAS Paper 89-001).

[3]Psiaki, M. L., and Martel, F., "Autonomous Magnetic Navigation for Earth Orbiting Spacecraft," *Proceedings of the 3rd Annual AIAA/USU Conference on Small Satellites* (Logan, UT), Utah State Univ., Logan, UT, 1989.

[4]Fox, S. M., Pal, P. K., and Psiaki, M. L., "Magnetometer-Based Autonomous Satellite Navigation (MAGNAV)," *Guidance and Control 1990; Proceedings of the Annual Rocky Mountain Guidance and Control Conference* (Keystone, CO), American Astronautical Society, San Diego, CA, 1990, pp. 369–382 (AAS Paper 90-051).

[5]Wertz, J. R. (ed.), *Spacecraft Attitude Determination and Control,* D. Reidel, Boston, MA, 1978.

[6]Jacobs, J. A. (ed.), *Geomagnetism,* Academic Press, New York, 1987.

[7]Bierman, G. J., *Factorization Methods for Discrete Sequential Estimation,* Academic Press, New York, 1977.

[8]Mook, M., private communication, Naval Research Lab., Washington, DC, Feb. 1988.

[9]Roy, A. E., *The Foundations of Astrodynamics,* MacMillan, New York, 1965.

[10]Gill, P. E., Murray, W., and Wright, M. H., *Practical Optimization,* Academic Press, New York, 1981.

[11]Langel, R., Berbert, J., Jennings, T., and Horner, R., "MAGSAT Data Processing: A Report for Investigators," NASA TM-82160, Nov. 1981.

[12]Psiaki, M. L., Martel, F., and Pal, P. K., "Three-Axis Attitude Determination via Kalman Filtering of Magnetometer Data," *Journal of Guidance, Control, and Dynamics,* Vol. 13, No. 3, 1990, pp. 506–514.